GFA Star Centroid Stability "Faint and Fat"
DESI-DOC 4030 v3

Mike Lampton with help from Stu Harris and Dick Joyce

October 31, 2018

Applicable Documents

Reil, K., et al., GFA System for BigBOSS, Proc SPIE 8450, 2012
DESI-0341-v1, Guide Star Density, K. Reil, October 2013
DESI-526-v6, GFA System Requirements, J.Silber, March 2017
DESI-1543-v1, GFA CCD Test Plan, R. Casas, Dec 2015
DESI-2420-v1, GFA Noise Requirements, M.Lampton, Nov 2016
DESI-2838-v2, GFA Unit Acceptance Criteria, S.Harris et al, June 2018
DESI-3223-v2, GFA Issues and SNR estimates, M.Lampton, Oct 2017
DESI-3603-v4, GFA Photon Transfer Curves, M.Lampton, April 2018
DESI-3644-v1, GFA Signal-to-Noise Ratio, M.Lampton, April 2018
DESI-3768-v1, PSF test in the GFA device, R. Casas, May 2018
DESI-4006-v7, Centroid Statistics with Noisy Images, M.Lampton, Sept 2018
DESI-4373v2, Bias, Dark, and Flat Fields, M.Lampton, October 2018
/global/projecta/projectdirs/desi/engineering/gfa/PreProductionCamera/Data/FATandFAINT
/global/projecta/projectdirs/desi/engineering/gfa/PreProductionCamera/Data/2018101-GFA5
/global/projecta/projectdirs/desi/engineering/gfa/PreProductionCamera/Data/99999999-GFA-FINAL

1 Introduction

DESI depends on the Guide Focus and Alignment system to provide accurate guiding of the Mayall telescope. A key performance requirement is that the centroid locations of star images accurately reflect image motion and must not be significantly perturbed by internal GFA disturbances. Here I examine a series of laboratory GFA "fat and faint" images taken on 2018 October 04.

2 Data Selection and Analysis

As part of a comprehensive study of GFA performance, J.Jimenez and R.Casas have explored the linearity, bias level, and flat field uniformity of these sensors. They gathered PSF data spanning a range of intensities, as part of the 2018 07/25 lab tests on GFA03 to see if image blooming occurs. More recently a sequence of images was obtained with GFA05, suitable to learn about centroid stability. This set is posted at NERSC directory shown above. The first two images are bias frames that determine the fixed pattern of individual pixel offsets. The remaining ten images contain the star signal in quadrant 3. From each image, I extracted a 40x40 pixel thumbnail centered on the spot (see Fig 1 below).

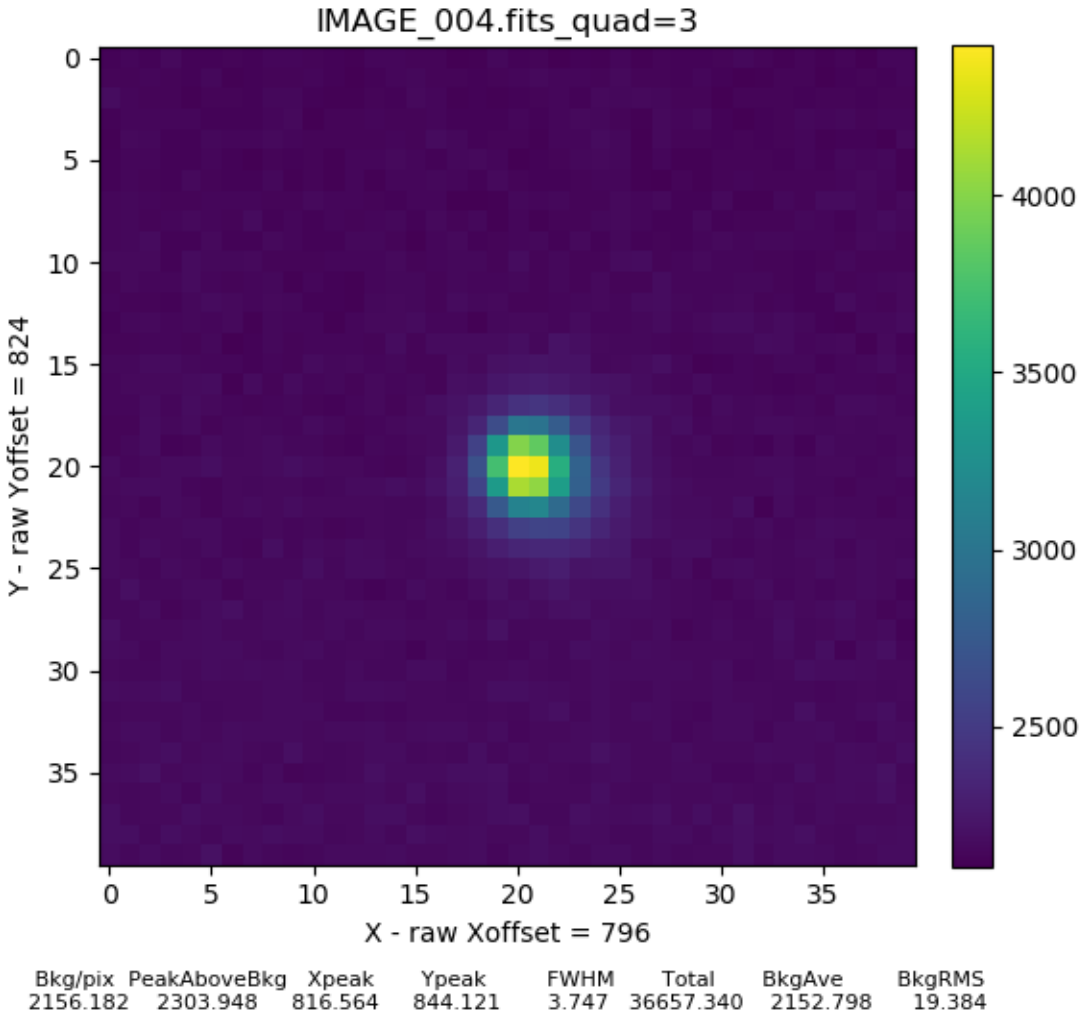

Figure 1: Typical 40x40 thumbnail image with its eight derived quantities; see text. This is one of ten non-bias-subtracted images. Bias subtraction reduces the constant offset and slightly modifies the noise level; see tables below.

To analyze these images for centroid stability, I extracted a 40x40 square thumbnail from each image, centered on the star peak. Within this thumbnail, I modeled the image as the sum of a uniform background (ADU) plus an added two dimensional Gaussian function whose parameters are peak height (ADU), Xpeak (pix), Ypeak (pix), FWHM (pix) and a derived parameter "Total" which is the volume of that best-fit Gaussian, in ADU sqPix. Statistics on these best-fit model parameters were gathered. In addition I divided each square thumbnail (1600 pixels total) into a central star zone (20x20 or 400 pixels) and a surrounding 1200 pixel background zone, from which I list BkgAve and BkgRMS, both in ADU. The Python code that I used in this work, `GFAv17.py`, is posted with this DESI-DOC. There, I use AstroPy for reading FITS files, and SciPy.optimize for access to its Levenberg-Marquardt nonlinear least squares fitter `curve_fit()`.

Bias frame subtraction can improve image homogeneity if the fixed pattern noise is significant, by reducing that source systematic error. However if only a few bias frames are averaged, this subtraction adds measurement read noise, increasing random error. I elected to use the average of the two bias frames in this sequence for subtraction, and also to analyze the frames without subtraction, to compare.

3 Results

The resulting derived fits to the ten star images are listed in Tables 1 and 2. Columns 2, 3, 4, 5 and 6 are five best-fit Gaussian parameters to each image. The "Total" column is the volume of that best-fit Gaussian, in ADU sqPix; it is an estimate of the total energy received during the exposure. Columns 8 and 9 give the average and rms statistics on the 1200 pixel background field in each thumbnail; their units are ADU per pixel. Beneath the ten rows of image data, I show two rows of column statistics: the parameter's column average and its column standard deviation. The column STDs are indicators of successive-frame time variation in the images, complementing the spatial (x,y) information within each image.

Table 1: Statistics of the ten "Fat and Faint" GFA Images, Bias Subtracted

Image	Bkg/pix	PeakAboveBkg	Xpeak	Ypeak	FWHM	Total	1200 Ave	1200 RMS
002	226.319	2421.338	816.576	844.113	3.639	36333.840	222.458	16.142
003	220.627	2374.759	816.580	844.100	3.673	36307.734	217.039	16.697
004	225.812	2383.223	816.567	844.119	3.682	36602.364	222.268	16.584
005	228.907	2392.124	816.566	844.115	3.659	36285.915	225.303	16.808
006	234.707	2369.898	816.543	844.079	3.684	36445.522	230.872	16.764
007	231.458	2332.535	816.541	844.073	3.730	36770.214	228.122	16.961
008	243.319	2219.559	816.494	844.023	3.829	36880.765	239.713	17.144
009	239.735	2212.946	816.479	844.003	3.828	36746.992	236.029	16.757
010	212.732	2248.784	816.471	844.004	3.780	36399.720	208.822	17.122
011	216.920	2229.920	816.465	844.005	3.806	36601.908	213.593	16.617
Col Aves	228.054	2318.509	816.528	844.063	3.731	36537.497	224.422	16.760
Col STDs	9.209	77.348	0.044	0.047	0.070	202.296	9.210	0.275

Table 2: Statistics of the same ten "Fat and Faint" GFA Images, Not Bias Subtracted

Image	Bkg/pix	PeakAboveBkg	Xpeak	Ypeak	FWHM	Total	1200 Ave	1200 RMS
002	2156.695	2417.888	816.573	844.115	3.644	36381.552	2152.989	19.180
003	2151.003	2371.363	816.578	844.102	3.678	36356.014	2147.570	19.578
004	2156.186	2379.702	816.564	844.121	3.687	36653.954	2152.798	19.384
005	2159.283	2388.762	816.563	844.117	3.664	36333.826	2155.834	19.882
006	2165.082	2366.559	816.541	844.080	3.689	36494.547	2161.403	19.970
007	2161.831	2328.996	816.538	844.075	3.735	36822.986	2158.653	20.563
008	2173.692	2216.486	816.491	844.025	3.835	36934.081	2170.243	20.377
009	2170.108	2209.893	816.476	844.005	3.834	36800.024	2166.560	19.670
010	2143.107	2245.790	816.468	844.006	3.785	36449.641	2139.352	19.093
011	2147.295	2226.954	816.462	844.007	3.811	36653.013	2144.124	19.085
Col Aves	2158.428	2315.239	816.526	844.065	3.736	36587.964	2154.953	19.678
Col STDs	9.208	77.161	0.044	0.047	0.070	204.314	9.210	0.494

From these data, it is clear that bias subtraction reduces the scatter in the background pixel contents, as it should since that scatter is caused, in part, by the sensor's systematic fixed pattern. The signal fit data however are not altered by bias subtraction.

The background noise level is 16 ADU rms, largely dominated by dark current. For example, at 500 electrons/sec.pixel and 5 seconds of exposure + readout, the shot noise would be 50 e rms or 14 ADU. This noise level is relatively homogeneous, not dominated by a few outliers, but rather is a broad Gaussian, as shown in the histogram below.

Pressing a bit farther into this background noise level issue, I examined the ten-point time sequence of each of the 1200 individual pixels, to learn their individual variances without regard to their neighbor's activity. These time sequences are therefore orthogonal to the spatial patterns quantified in Tables 1 and 2 above. They are immune to spatial gradients but of course are sensitive to time trends in the background level. Tables 1 and 2 do not show much, if any, such trends.

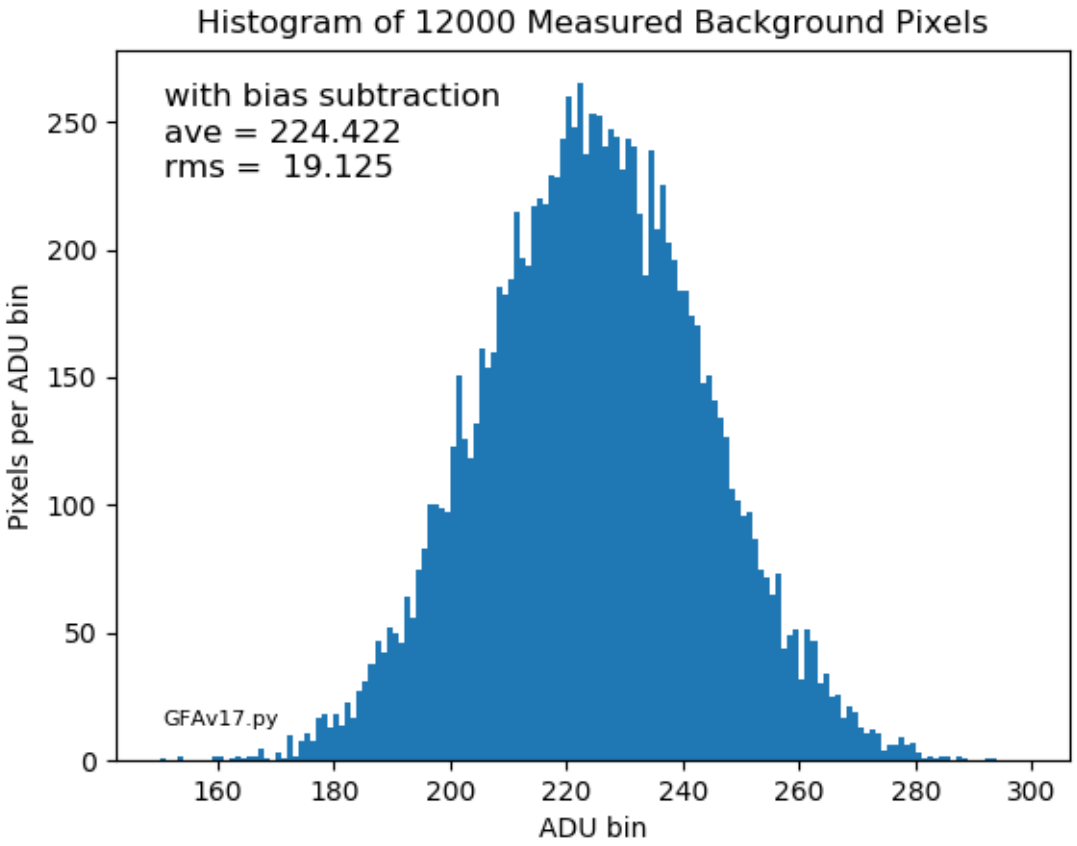

Figure 2: Histogram of thumbnail background pixels for all ten images, 1200 x 10 = 12000 samples. These are from the bias-subtracted set. Their aggregate spread is 19 ADU, somewhat larger than the individual frame background spreads of 17 ADU as shown in Table 1 column 9 average. This extra spread may be caused by slight trends in the data sequence. The non-bias-subtracted set is similar but has a slightly larger breadth, 22 ADU, and is shifted to higher values of ADU, around 2156.

Statistics of these individual pixel time sequence stacks are shown in the listing below. Units of averages and rms's are ADU; variances are ADU**2, and var(var) are ADU**4:

```
aveStackAVE=   224.422
rmsStackAVE=    10.279
varStackAVE=   105.657

aveStackRMS=    15.719
rmsStackRMS=     3.613
varStackRMS=    13.051

aveStackVAR=   260.126
rmsStackVAR=   115.565
varStackVAR= 13355.253
```

Here, from `aveStackRMS` we see that the typical ten-point pixel sequences scatter in time by about 16 ADU, explaining nearly all of the observed total background scatter.

The key finding from this analysis is that the test images have stable but noisy background, and reveal trends in the image intensity: the central peak intensity declines by 8 percent over this ten-image run, while its FWHM increases by 4 percent. Its total signal intensity, or volume in ADU sqPix, remains roughly constant. So, this trend appears to be a slight defocus over time with the net light flux remaining constant. The best-fit peak locations both trended downward by about 0.1 pixels during this run.

All these effects are most likely caused by the test setup and should not be attributed to an instability of the GFA. To properly address the issue of guide star stability, I have de-trended the centroid locations as shown in Figure 3 below. Both slopes are about -0.015 pixel per image. Correcting for these trends gives us RMS deviations of 0.012 and 0.018 pixels, a factor of three smaller than the uncorrected 0.044 and 0.047 pixel errors obtained in Tables 1 and 2. These locations, and their trend lines, are plotted in Figure 3 below.

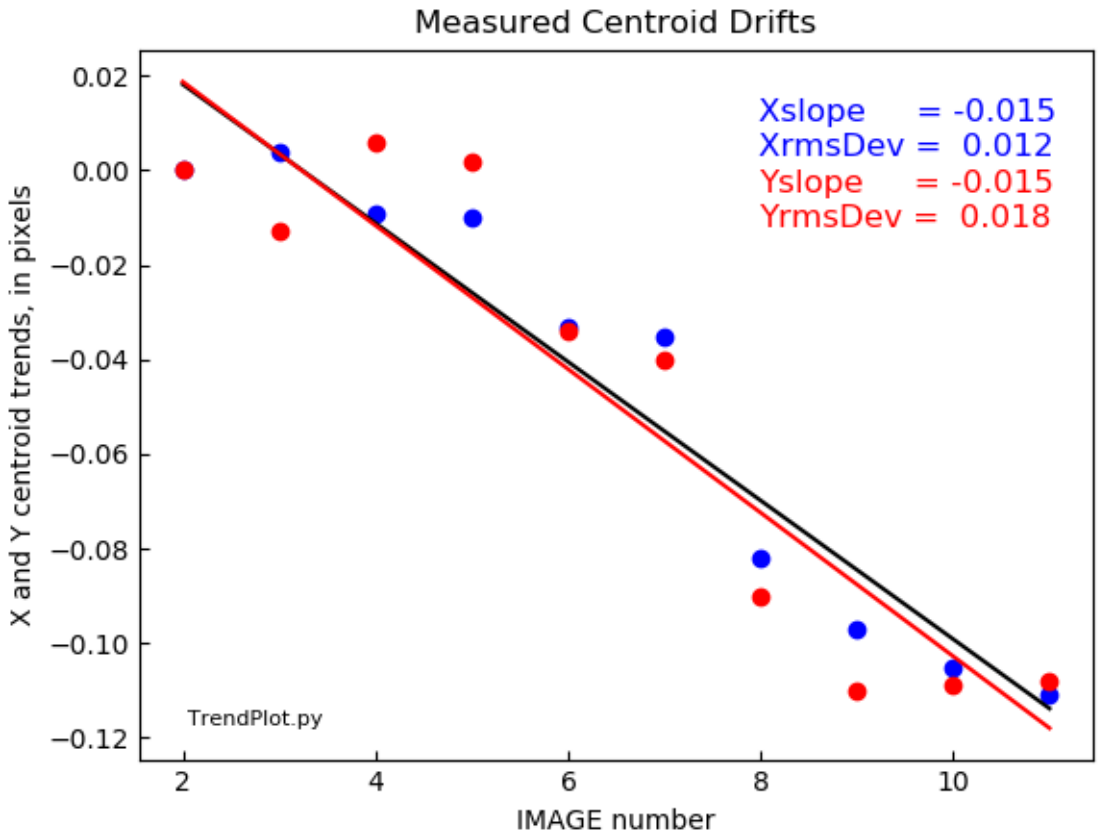

Figure 3: Trends in centroid locations from Table 1 above. Shown are the straight line fit slopes and the rms deviations of the measured centroids from these slopes.

The peak intensity trend from Tables 1 and 2 is plotted in Figure 4 below, along with its best fit linear trend. With this trend removed, the RMS peak variation becomes 33 ADU, a big reduction from the 77 ADU without trend removal.

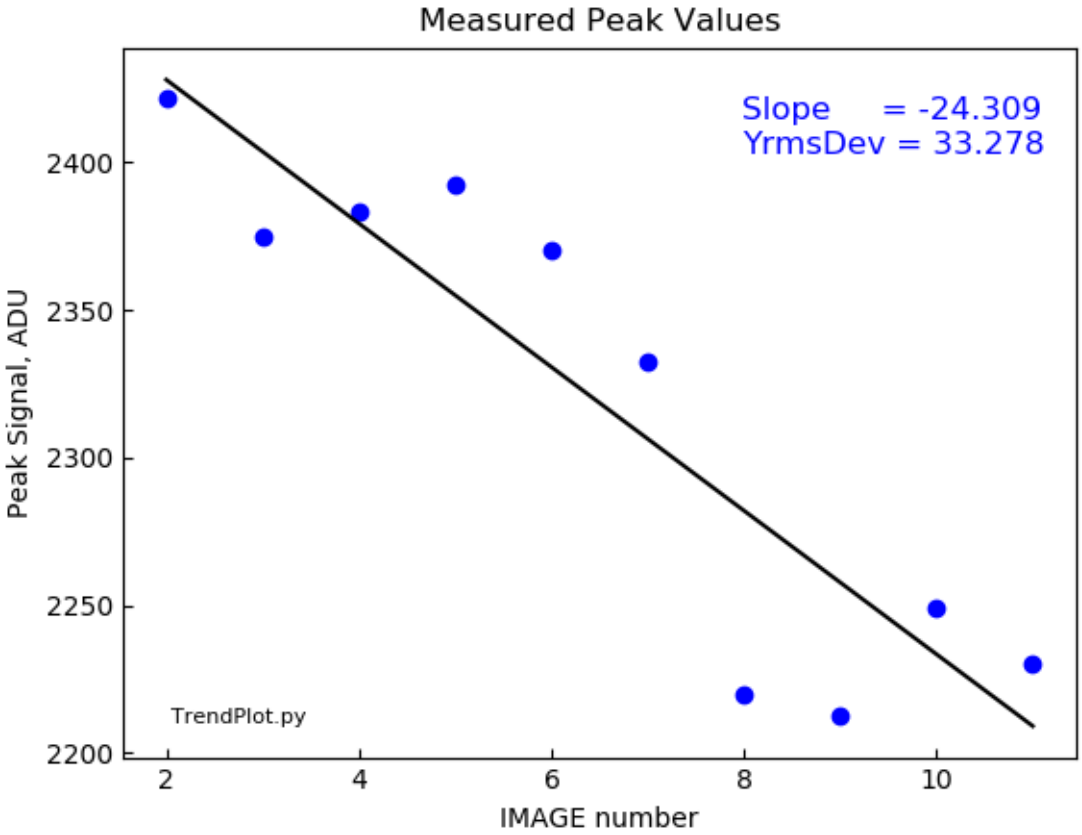

Figure 4: Peak signals from Table 1 are plotted; also shown is the straight line fit slope and the rms deviation from this best fit slope. It is possible that significant peak flux errors are present even after de-trending: focus variations could in principle cause this.

4 Extrapolation to Mountain Performance

With these test data in hand, what can we predict for guide performance on the mountain? To be quantitative, the first step is to convert the lab data into mountain equivalent data. Here I use the assumptions in `Guider-SNR-v51.xlsx` than contains specifics on the Mayall, the GFA bandpass filter, the sensor chip, the exposure time, and the various noise contributions.

```
GAIN      = 0.274   # ADU/electron, R. Casas report
DARK      = 65.6    # electron/pix/second, R.Casas report
READ      = 16.8    # electrons RMS, R.Casas report
OFFSET    = 200     # ADU no bias subtracted
NIGHTSKY  = 16.0    # electrons/pix/second, moon=7days
PIXARCSEC = 0.214   # plate scale 70 microns/arcsec
TOBS      = 1.0     # second exposure
FWHM      = 3.74    # observed PSF, pixels
PEAKADU   = 2270    # gives Rmag=14.00
```

With these values, the expected background noise level is composed of read noise (17 electrons rms) and the Poisson shot noise from dark current and night sky (sqrt(66 + 16) = 9 electrons rms) whose RSS is 20 electrons or about 6 ADU. For the following discussion I regard 6 ADU rms as a realistic "cold case" noise level. Our present data have about three times this noise level, 16 ADU rms, which I regard as a typical "hot case" noise level.

With a given noise level, a given star, a given seeing, what would we expect from a guider centroid error distribution? The rms errors in x or y are usually predicted by the astrometric error formula (see for example Monet et al[1]) given by the expression

$$Xrms = Yrms = 0.5\ \frac{FWHM}{SNR} \tag{1}$$

where $FWHM$ is the image spot size and SNR is the star image signal-to-noise ratio. This formula is applicable at low signal levels where the noise is sensibly uniform over the image, with the star shot noise being negligible in comparison with the other noise contributions. For brighter stars, the shot noise in the starlight worsens both the star signal and its noise level, and this formula continues to apply provided that "noise" includes both the sky noise and the star shot noise. My recent analysis (DESI-4006v7) shows that the coefficient in this formula depends slightly on the shape of the star image, being closer to 0.6 for Gaussians and 0.7 for Moffat profiles commonly used to describe seeing.

[1]Monet, D. G., et al., "Preliminary Astrometric Results from KEPLER," arXiv 1001.0305 (2010)

SNR from Total Flux: Given a best fit Gaussian FWHM and Peak, he total flux of starlight in one exposure is $Total = (\pi/4ln2) \cdot Peak \cdot FWHM^2$. For a succession of exposures, the noise is just the RMS scatter among this population of Totals. This method avoids defocus trending errors but is still susceptible to total intensity variations between exposures. Total fluxes are reported in Tables 1 and 2 column 7: $Peak = 36550\ ADU$, $RMS = 203\ ADU$ giving $SNR = 180$. Column 6 gives $FWHM = 3.73\ pixels$. From Monet:

$$Xrms = Yrms = 0.0104\ pixel = 0.0022\ arcsec \tag{2}$$

SNR from 50/50: A crude way to estimate the SNR of a peak is to compare the 50 percent encircled energy signal $S50$ against the noise $N50$ in the $EE50$ circular patch around the peak. This method does not need a succession of images: it applies to any single measurement. By definition, energy is just half the total energy in the spot: $S50 = 0.5{*}Total$. The noise variance is the sum of background and signal shot noise, so let $Npix50$ represent the number of pixels in the EE50 circle, $(\pi/4) * FWHM^2$. With individual pixel background noise of $Brms$, the background variance is $Npix50 * Brms^2$ with units of ADU^2. The shot noise variance in EE50 is $Gain * S50$. Hence:

$$SNR_{50} = \frac{S50}{N50} = \frac{S50}{\sqrt{Npix50 * Brms^2 + Gain * S50}} \tag{3}$$

For our lab evaluations, Brms=16ADU, Gain=0.274 ADU/e, FWHM=3.73 pixel, N50=11 pixels and S50= 18300 so $SNR_{50} = 207$. Applying Monet's rule we expect

$$Xrms = Yrms = 0.0091\ pixel = 0.0019\ arcsec \tag{4}$$

In Table 3 below I summarize the findings of this section. Our measured centroid location errors may be somewhat larger than their truly random jitter owing to lab equipment trends that are more complicated than linear. The linear-trend-removed figure, 0.015 pixels RMS is then an upper limit to the true value, which could plausibly be as low as 0.010 pixels RMS. This figure compares well with the expectations from the random-noise-limited Monet rule, which gives about 0.010 pixels for our signal level. From these data I conclude that we are demonstrating X and Y centroid random location errors of 0.01 to 0.015 pixels RMS.

Table 3: Summary of SNR and Centroid Position Error Distribution

Method	Basis	X or Y rms pix	X or Y rms arcsec
Measured Centroids	Raw location fits	0.045	0.0096
Measured Centroids	Linear de-trended fits	0.015	0.0032
Predicted from Monet	Total, SNR = 180	0.0104	0.0022
Predicted from Monet	50/50, SNR= 207	0.0091	0.0019

5 Simulated Centroid Error Distribution

To extrapolate our lab data to fainter magnitudes and poorer seeing, I wrote a simple star field thumbnail simulator, 40 x 40 pixels, that includes a choosable uniform background noise level plus an adjustable 2D circular Gaussian peak contributing star signal and Poisson shot noise. My motive here is to better understand guider errors in the realm of fainter stars which will be needed in our higher Galactic latitude survey regions, and poorer seeing, which can happen any time.

Sanity check: To verify the simulator's noise properties, I ran a photon transfer curve of the pixel (number 780) that lies nearest the peak in the 1600 pixel field, examining 100 successive thumbnail exposures at each of 40 intensity levels. I chose two levels of noise: 6 ADU rms as our "cold case," and 16 ADU rms representative of our "hot case." Results are shown in Figure 5. They look as expected; in particular the slope of variance vs mean is 0.29 ADU/electron, close to the 0.274 ADU/electron baselined in the model.

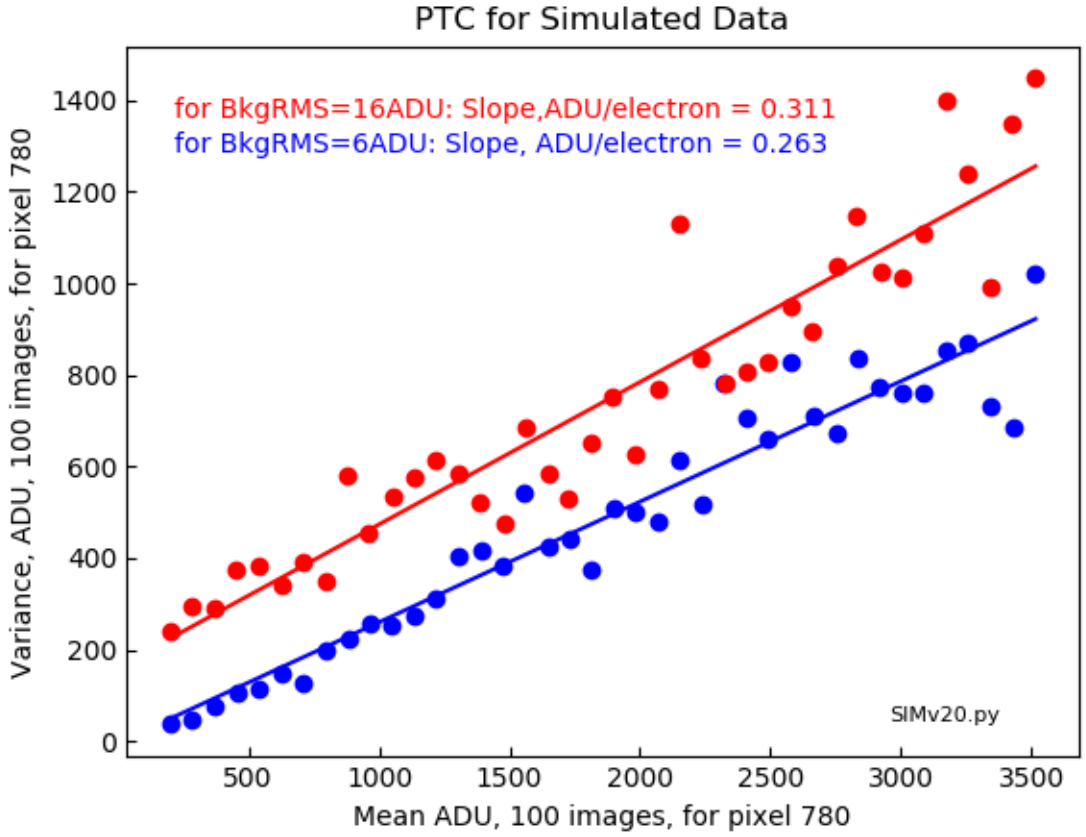

Figure 5: Photon Transfer Curve for simulated Gaussian PSFs atop a flat but noisy field. Test pixel is number 780, closest to the Gaussian peak. Each datum plotted is the average variance vs average signal for 100 images. 40 such sets are run with intensity levels spanning zero to 3900 ADU peak value. Two background noise levels are plotted: 6 ADU rms (Rn=19 e rms plus other contributors), and the higher value of 16 ADU rms as found in Table 1 above. Other exposure constants (Texposure, night sky, gain, etc.) are taken from `Guider-SNR-v51.xlsx`.

Simulated Centroid Location Errors

To obtain a well-calibrated set of ceNtroid location errors, I ran 100 image iterations for the two noise cases, two seeing cases, and nine star signal levels. I report these results in Figure 6. The simulator employed was `SIMv23.py` whose source code is included in this DESI-DOC release. The two sky conditions are good seeing at 0.8 arcseconds FWHM, and poor seeing at 1.6 arcseconds FWHM. For almost all conditions simulated, the predicted GFA performance would allow satisfactory guiding on a single star in a single GFA.

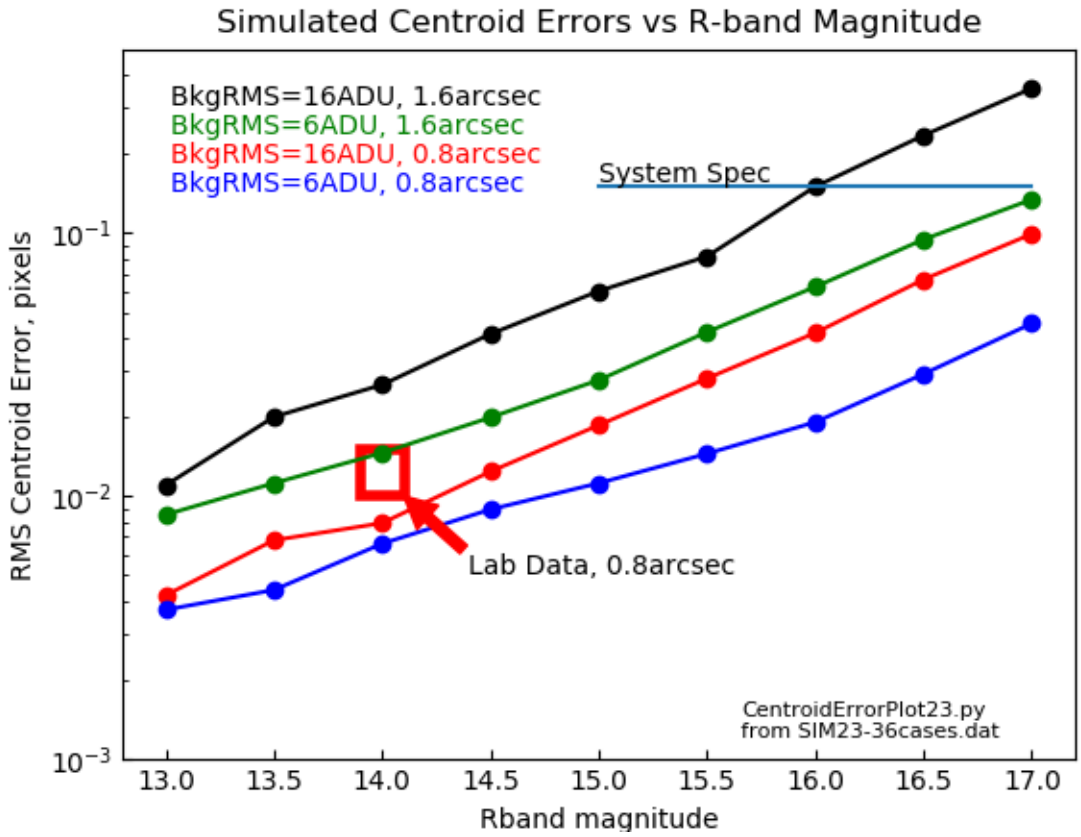

Figure 6: The simulator allows us to extend the lab data (**box**) towards fainter magnitudes and poorer seeing conditions. Here I use 100 exposures per simulated data point to gather its mean and standard deviation statistics. The simulation at its high-noise, excellent-seeing settings closely matches the lab data. Here the simulations are run for a one-second exposure time, to match the lab data. The horizontal bar "System Spec" is 0.03 arcsecond rms or 0.15 pixel rms; it applies to the entire guider system, which supplies additional guide star averaging and smoothing.

6 Comparison with Requirements

The DESI Project carries requirements on the GFA System to achieve 0.03 arcseconds RMS at an update rate of 0.2 Hz, with a latency less than 3 seconds as shown in Figure 7.

from DESI-0810v6 FPS Requirements

IN.FPA-2001	Guide Centroid Accuracy	The FPS shall deliver a tracking error signal better than 0.03 arcseconds, at an update rate of 0.2 Hz, and latency less than 3 seconds.	The Mayall telescope can meet its pointing requirements with this accuracy of guide signal. For commissioning and debugging a much higher precision and update rate is advantageous. (DESI-0315)	A,T	Simulate/analyze available guide stars and performance of guide sensors. Verify on-sky.

from DESI-0526v6 GFA Requirements

IN.AATP-40000	GFA Guide Centroid Accuracy	The GFA system shall be capable of delivering a tracking error signal to the TCS better than 0.03 arcseconds rms.	The Mayall telescope can meet its pointing requirements with this accuracy of guide signal. (DESI-0315). See IN.AATP-40032 for timing requirement.	A T	This will need on sky calibration.

Figure 7: Requirements on GFA performance flow down from the Focal Plate System.

This requirement is vague. Should it apply at new moon? full moon? good seeing? poor seeing? bright stars? High Galactic latitude faint stars? Perhaps the worst combination of these? This vagueness makes it difficult to decide if our GFA hardware will meet its requirement.

The "System" surely refers to the six guide GFAs, most of which, with most observing conditions, will have usable guide stars. Our GFA test data were equivalent to bright star conditions (Rrmag=14) with excellent seeing (0.8 arcseconds). These data show 0.002 arcseconds RMS (0.01 pixels RMS) guide errors in any single one-second exposure, by far beating our requirement.

Simulated extrapolations to fainter stars and poorer seeing suggest that our requirement will continue to be met down to Rmag =16 even with poor seeing snd ons single guide star. Longer exposures (2 to 5 seconds) will certainly improve this performance further. Capturing several guide stars on several GFAs will deliver even more guide accuracy.

How faint will we need to go? Rmag=14 stars are rare at high Galactic latitudes where many of our targets lie. An study by Kevin Reil (Figure 8 below) quantifies the guide star field densities at high Galactic latitudes. From that study it appears that getting to Rmag=16 should suffice. If my extrapolations are correct, this should be easily accomplished with our current GFA design.

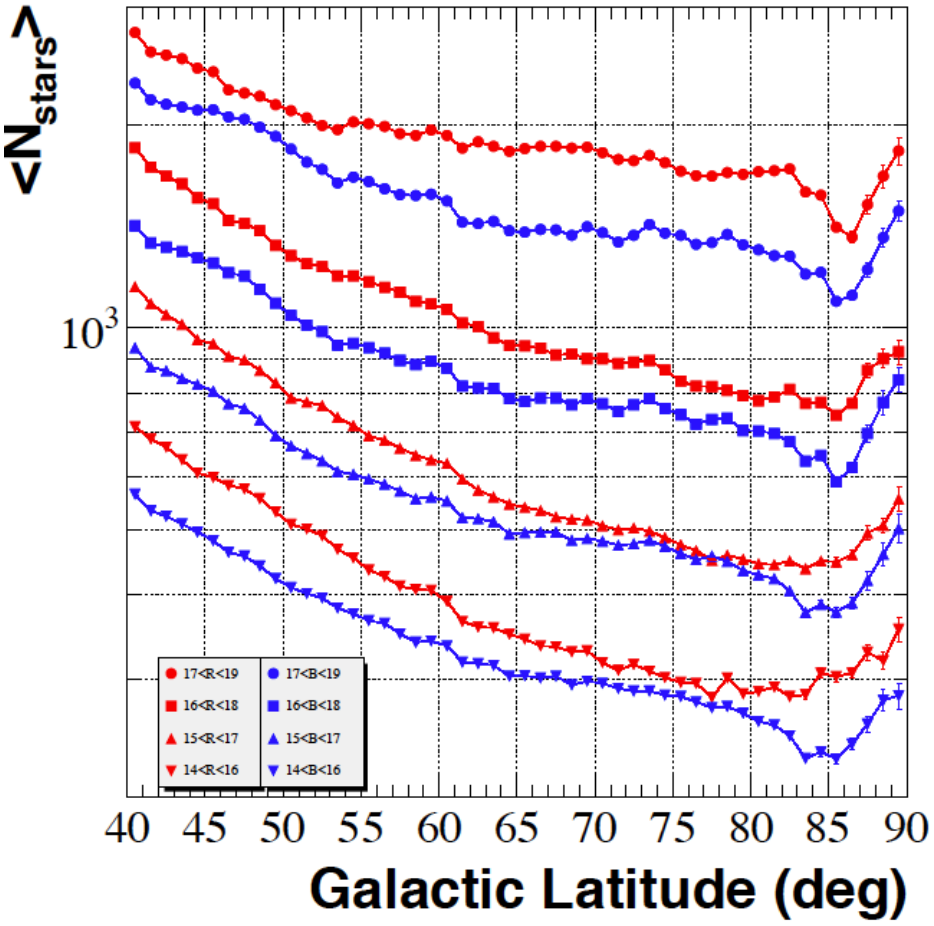

Figure 8: Star counts per square degree as a function of Galactic latitude, from Reil et al 2012. The GFA area of $400mm^2$ is a sky area of 0.006 square degrees, so a star density of 160 would average one star per GFA. The minimum of this curve for stars in the 14 to 16 Rmag group is at 300 stars per square degree, and so most fields will deliver one or two stars of at least R=16mag to each GFA, anywhere on the sky.

7 Issues Not Studied Here

Dark-time Magnitude Limit: The choice of star fields for DESI is driven by the need to cover the sky as completely and deeply as will maximize the yield of distant galaxies and QSOs. To accomplish this task there is considerable freedom to nudge each chosen field so as to guarantee that a few good guide stars are visible to our GFAs. It may well be possible to perform the entire DESI dark-time survey, including our high Galactic latitude fields, without having to guide on anything fainter than (say) R=15 or even 14. Progress on this question will have to come from our mission planners. Actual experience from the DEC program could help inform our planning.

Bright-time Magnitude Range: For those portions of the lunar month that produce a bright sky all night, the target fields will naturally focus on brighter targets, and these are found at lower Galactic latitudes where guide stars are more plentiful. This requirement may not place any new requirements on the performance of individual GFAs other than the freedom from bright star overload — which again can probably be managed by careful field selection. My "cold case" results are for a moon age of 7 days, half-moon above the horizon, but this night sky level contributes only a small portion of the total cold case noise. I have not explored this issue but again the DEC experience could help inform our planning.

Seeing Wobble Although the largest component of star twinkling is an apparent rapid fluctuation in intensity, seeing also produces a centroid position wobble that I have not included here. Wobble should average out over long exposures, but not at short exposures, so there is a position noise spectrum to understand. Perhaps someone on our team could contribute a recommendation.

Choices of Readout Cadence: Six GFAs can operate in a round-robin manner, each delivering a guide signal vote (say) once per second, easily meeting the cadence requirement, yet allowing six seconds for exposure + readout. Longer exposures are of course helpful in gaining guide accuracy on fainter stars but are unnecessary on brighter field stars. I have not explored this issue.

Focussing: The GFAs must deliver sufficient signal to noise ratio that the defocused donuts are accurately measurable. I have not studied this requirement. There are years of practical experience from the DEC program with which to compare.

PID Filtering: Our high level system requirements bear on on system performance, and guiding is traditionally done by passing the guide star deviation signals through a "PID" controller whose job is to optimally combine Proportional, Integral, and Differential time operators in such a way as to maximize guide accuracy. I have not studied this issue. Again, there are years of practical on-mountain DEC experience with which to compare.

8 Conclusion:

Test data on GFA 05 show excellent guide star centroid location stability, of the order of 0.01 pixel RMS (two milliarcseconds rms!) for a bright, well-focussed spot. The system level requirements on guiding accuracy apply for some range of seeing and star magnitude. Extrapolating the test data to fainter stars, and to poorer seeing, shows that the system-level requirement is likely to be met, depending on its interpretation of the requirement. I caution that my tiny simulator, used for these extrapolations, has not been validated with on-sky tests.

–end–